Leonardo R. OLIVEIRA[1], Tárcio A. S. BARROS[1], Paulo S. NASCIMENTO Fo.[1] , Marcelo G. VILLALVA[1], Ernesto RUPPERT[1]

Universidade Estadual de Campinas (1)

doi:10.15199/48.2015.09.64

Grid-tie pv microinverter with isolated full-bridge boost converter controlled with the state-space feedback control method

***Abstract**. This paper presents the modeling and control design of an isolated full-bridge boost converter fed by a photovoltaic (PV) device. The converter and PV device are modeled using the method of average state variables and the controller is designed with the state-space feedback control technique, using concepts of characteristic polynomial, controllability and Ackerman's matrix. The dynamic model of the converter is obtained and the voltage controller is designed in order to achieve the regulation of the input voltage of the boost converter, thus allowing the direct control of the PV voltage, which brings advantages when this system is compared to traditional control strategies for grid-tie PV converters.*

***Streszczenie.** W artykule zaprezentowano modelowanie i projekt sterowania izolowanym pełnomostkowym, przekształtnikiem typu boost zasilanym przez ogniwo fotowoltaiczne. Zbadano właściwości dynamiczne. Układ sterowania jest tak zaprojektowany żeby osiągać prawidłowy poziom napięcia. **Pełnomostkowy przekształtnik typu boost sterowany sprzężeniem zwrotnym typu state-space stosowany do współpracy z ogniwem fotowoltaicznym**.*

Keywords: Boost converter, state space control, pv microinverter.
Słowa kluczowe: przekształtnik typu boost, ogniwo fotowoltaiczne.

Introduction

Due to the forthcoming world energy crisis caused by the imminent exhaustion of fossil resources, besides the environmental damages associated with the exploitation of non-renewable sources, renewable energy sources began to be used as a way to diversify the energy supply of many countries [1].

Within this context, the distributed generation of electricity using photovoltaic (PV) solar panels as a primary source is an excellent alternative for Brazil due to its great solar potential. The lowest irradiation rates in the Brazilian territory are near 4,500 Wh/m^2/day at the very southern extreme and rates as high as 6,000 Wh/m^2/day may be reached in the northern regions near the Equator.

The exploitation of the PV source requires static power converters for the conversion from DC to AC and the injection of power into the grid according to requirements of energy quality, synchronization and safety. Many different converter topologies for this purpose can be found in the literature [2-9]. For low-power microinverters in the range of 250 W high-frequency isolated topologies are preferred since they avoid bulky low-frequency transformers at the connection with the grid, thus increasing efficiency and reducing equipment size and weight.

This work presents an input-regulated isolated boost converter aimed as a first conversion stage in grid-tie PV microinverters. The regulation of the input voltage of DC converters applied to grid-tie systems reduces voltage ripple at the output of the PV source and makes easier the implementation of faster and more accurate maximum power point tracking (MPPT) strategies by increasing sampling rate and reducing the amplitude of voltage perturbations. The input voltage regulation has been proven in previous works to increase the overall efficiency of PV systems based on other topologies of converters.

Full-bridge boost DC-DC converter

The full-bridge boost converter used in this work is intended to be used as the first stage of a grid-tie inverter based on the classical converter topology which combines a DC-DC converter cascaded with a DC-AC inverter.

The DC-DC isolated boost is used to step up the voltage of the PV module (usually in the range of 30 V – 40 V for 60-cell crystalline modules) and deliver power to the DC link which interfaces with the next stage. The DC link is modeled as a constant voltage source V_0, as shown in Figs. 1 and 2.

The isolated full-bridge boost is a well known converter [11] used in many applications of switching power supplies, where the output voltage is usually controlled. This paper proposes a different usage for the full-bridge boost converter where the input voltage is regulated and its output voltage is kept constant and regulated by the second conversion stage.

In grid-tie PV systems the regulation of the PV voltage is necessary for achieving maximum system efficiency with MPPT algorithms. The output current or voltage of the PV module may be regulated for tracking the maximum power of PV modules [10, 12, 14], however voltage regulation requires less control effort and allows better accuracy, since the operating current of PV modules changes randomly and significantly with the irradiance [W/m^2] of sunlight, while the maximum power voltage of PV modules depend on the temperature only. Temperature changes are slower than irradiance disturbances during the normal operation of PV systems. However regulating the PV voltage as proposed in this work requires special attention because modeling and controlling the input voltage of the boost converter is unusual and depends on the characteristics of the PV device.

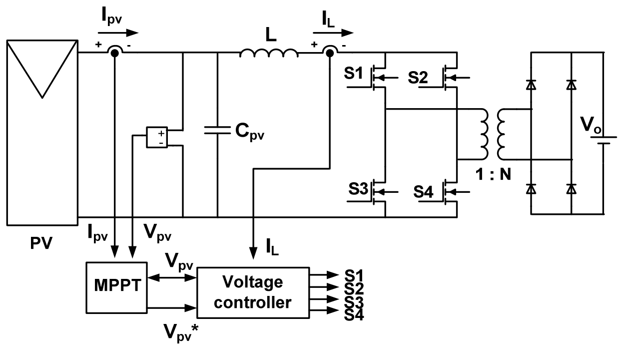

Fig. 1. Full-bridge isolated boost DC-DC converter interfacing the PV module with the DC link represented by the voltage source V_0, which may be the input voltage of a cascaded DC-AC inverter.

Figure 1 shows the full-bridge boost converter fed by a PV module. The input voltage of the converter is regulated by a voltage controller that senses the converter input current on the boost inductor L and the input voltage on the capacitor C_{pv}. One great advantage of the converter input voltage regulation is the reduction of the capacitor C_{pv} size due to the attenuation of the voltage ripple at the output of the PV module by action of the feedback controller.

In Fig. 1, the voltage reference V_{pv}^{*} is generated by the MPPT algorithm with the objective of maximizing the power generated by the PV system. Several MPPT algorithms have been proposed in the literature and the study of this subject is not in the scope of this work. In the simulations

The "perturb and observe" (P&O) method was used [10, 13]. This method is a well known MPPT strategy used in many commercial PV inverters due to its simplicity, ease of implementation, low cost, and satisfactory results for stationary PV systems where sudden irradiance changes are not usual.

The reference voltage is compared with the actual PV voltage V_{pv} and the error signal is processed by the state-space feedback voltage controller. The output of the voltage controller determines the duty cycle of switches S1-S4 of the full-bridge inverter. The switches are controlled by a pulse width modulation (PWM) generator, now shown in Fig. 1 for simplicity, which compares the output signal of the voltage controller (modulation signal) with a triangle wave (modulation carrier).

The focus of this work is the design of the linear compensators used in the voltage controller. The design starts with the modeling of the system composed of the PV module and the full-bridge converter. The system model has the state variables V_{pv} and I_L and the input variables d, which is the duty cycle of the full-bridge boost switches. The system modeling and control design are explained in next sections.

Full-bridge boost converter modeling

The method of average state variables presented in references [12, 15] is used. Fig. 2 shows the average voltage and currents of the PV system with the full-bridge converter. The PV module is replaced by a linear model with $\mathrm{V_{eq}}$ and $\mathrm{R_{eq}}$, i.e. its equivalent voltage and resistance at the maximum power point (at 1,000 W/m2 and 25 °C) [10, 12, 14, 16].

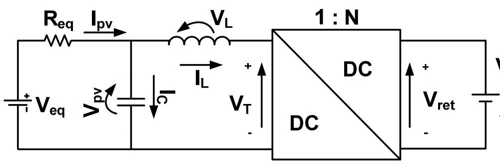

Fig. 2. Linear model of the PV module and boost converter with average voltages and currents. The transformer ratio of the original boost circuit is represented by the 1:N ratio DCDC transformer.

The high-frequency switching ripple of voltages and currents are eliminated when average variables are used. Only the low-frequency natural behavior of the system is analyzed with the average circuit model of Fig. 2 [12].

In the continuous mode of operation the output voltage of the boost converter is given by [15]:

(1) $$V_o = N\frac{V_{pv}}{2(1-D)}$$

By replacing (1-*D*) by *d* and V_{pv} by V_T one finds:

(2) $$V_T = \frac{V_0}{N}.2d$$

With Kirchhoff's Voltage Law one can write

(3) $$R_{eq}.I_{pv} + V_{pv} - V_{eq} = 0$$

(4) $$V_L + V_T - V_{pv} = 0$$

From (4):

(5) $$\frac{dI_L}{dt} = \frac{V_{pv}}{L} - \frac{V_0}{LN}.d$$

From Kirchhoff's Current Law on the PV equivalent model:

(6) $$I_{pv} = I_C + I_L$$

By replacing (6) in (3) and isolating the derivative of V_{pv}

(7) $$\frac{dV_{pv}}{dt} = -\frac{V_{pv}}{R_{eq}.C} + \frac{V_{eq}}{R_{eq}.C} - \frac{I_L}{C}$$

From (5) and (7), by neglecting the perturbation V_{eq} one can write the state space equation bellow, where the PV voltage and the inductor current are the state variables

$$\dot{x} = Ax + Bu\,;\; Y = C$$

(8) $$\begin{bmatrix}\dot{V_{pv}}\\ \dot{I_L}\end{bmatrix} = \begin{bmatrix}-\frac{1}{R_{eq}.C} & -\frac{1}{C}\\ \frac{1}{L} & 0\end{bmatrix}.\begin{bmatrix}V_{pv}\\ I_L\end{bmatrix} + \begin{bmatrix}0\\ -\frac{V_0}{L.N}\end{bmatrix}.d\;;$$

$$Y = \begin{bmatrix}1 & 0\end{bmatrix}.\begin{bmatrix}V_{pv}\\ I_L\end{bmatrix}$$

The values of the circuit parameters are replaced in equation (8) for a quantitative analysis of the dynamic system. The input capacitance C was chosen for a reduced voltage ripple. The value of the output voltage V_0 is greater than the peak of the grid voltage intended for the grid-tie inverter that will be cascaded to the boost converter, thus allowing the power flow from the DC link to the grid. The 1:N transformer ratio was chosen to make to output voltage of the PV module compatible with the input voltage of the transformer. The inductance L was chosen in order to reduce the current ripple on the inductor, consequently reducing the PV module current ripple. The value of L also was chosen in order to keep the converter in the continuous current mode of operation [12]. The value R_{eq} was obtained for the Bosch M2403BB monocrystalline solar panel using the modeling method explained in [10, 17]. With equation (8) and the parameters :

(9) $$\begin{bmatrix}\dot{V_{pv}}\\ \dot{I_L}\end{bmatrix} = \begin{bmatrix}-3.87 & -10^3\\ 500 & 0\end{bmatrix}.\begin{bmatrix}V_{pv}\\ I_L\end{bmatrix} + \begin{bmatrix}0\\ -25.10^3\end{bmatrix}.d$$

Controller design

The state-space feedback control technique from [19-20] is used for designing the compensators of the voltage controller. The dynamic behavior of the linear system in (9) depends of the location of poles in the complex plane. The objective is to design compensators that will reallocate poles and make the system behave according to the desired characteristics.

The complete system with state feedback control is shown in Fig. 3. The values of K (matrix) and K_i (constant) are given by the matrix K_a containing the feedback gains. This matrix was obtained with Ackerman's method given by equation (10):

(10) $$\mathrm{K_a} = [\mathrm{K} \,\vdots\, -\mathrm{K_i}] = [0\;0 \ldots 0\;1].\varrho^{-1}.\mathrm{Pc}(\mathrm{A_a})$$

The first design step is to find the characteristic polynomial of the system which contains the dominant poles. The characteristic polynomial P_c of a second-order system is determined by equation (11).

(11) $$\mathrm{S_{1,2}} = -\xi\omega_n \pm j\omega_n.\sqrt{1-\xi^2}$$

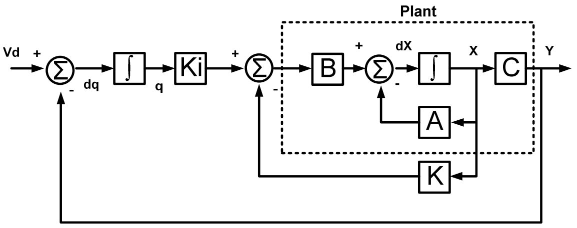

Fig. 3. Complete system with state feedback control.

The values of the natural frequency ω_n and dumping factor ξ are obtained from (12) and (13) [19,20]. The maximum overshoot M_o is chosen by the designer and the settling time t_{set} is chosen based on the constant time of the system.

(12) $$\xi = \frac{-\ln M_O}{\sqrt{\pi^2 + \ln(M_O)^2}}$$

(13) $$\omega_n = \frac{4}{\xi . t_{set}}$$

The original 2nd order system becomes a 3rd one with the addition of an integrator in the feedback loop. The order increase requires the addition of an auxiliary pole α_1 that must be chosen to be faster than the dominant poles. Thus the characteristic polynomial will be:

(14) $$P_c(s) = (s + S_1).(s + S_2).(s + \alpha_1)$$

Next step is finding the augmented matrices $\boldsymbol{A_a}$and $\boldsymbol{B_a}$. This is achieved by modifying the matrices of equation (9) as shown below:

(15) $$\dot{x_a} = A_a.x + B_a. \quad ; \quad \begin{bmatrix} \dot{x} \\ \dot{q} \end{bmatrix} = \begin{bmatrix} A & 0 \\ -C & 0 \end{bmatrix} . \begin{bmatrix} x \\ q \end{bmatrix} + \begin{bmatrix} B \\ 0 \end{bmatrix} . u$$

From (15), the augmented matrices are:

(16) $$[A_a] = \begin{bmatrix} -3.87 & -10^3 & 0 \\ 500 & 0 & 0 \\ -1 & 0 & 0 \end{bmatrix}$$

(17) $$[B_a] = \begin{bmatrix} 0 \\ -25.10^3 \\ 0 \end{bmatrix}$$

Ackerman's method requires the inverse of the matrix of controllability (ϱ) calculated with equation (18):

(18) $$\varrho = \left[B_a \,\vdots A_a . B_a \vdots \ldots A_a{}^{m-1} . B_a \right]$$

Now *m*=3 in this 3rd order system obtained with the addition of the integrator. From equation (18) one obtains the controllability matrix of equation:

(19) $$\varrho = \begin{bmatrix} 0 & 25.10^7 & -9675.10^5 \\ -25.10^3 & 0 & 125.10^9 \\ 0 & 0 & -25.10^7 \end{bmatrix}$$

The inverse of the controllability matrix is given by equation (20) below:

(20) $$\varrho^{-1} = \begin{bmatrix} 0 & -5 & -2.10^2 \\ 4.10^{-9} & 0 & 15{,}48.10^{-9} \\ 0 & 0 & -4.10^{-9} \end{bmatrix}$$

The poles of the characteristic polynomial are obtained with (12) and (13). The maximum allowed overshoot is arbitrarily chosen $M_O = 1$. The resulting dump ratio is approximately ξ=0.82. The settling time t_{set} is calculated with the equation:

(21) $$t_{set} = \frac{L}{30.R_{eq}}$$

The substitution of (21) in (13) results the natural frequency 11,592.509 rad/s. With the natural frequency and dump ratio determined previously, the dominant poles are:

(22) $$S_{1,2} = -1.8\ 10^3 \pm j1.22\ 10^3$$

An auxiliary pole of half the frequency of the dominant poles was chosen for the determination of the characteristic polynomial P_c. After obtaining the values of P_c, the values of matrix $A_a$are inserted in (14), which results equation (23) below:

(23) $$P_c(A_a) = \begin{bmatrix} -1.89.10^{10} & -1.26.10^{11} & 0 \\ 6.39.10^9 & -1.88.10^{10} & 0 \\ 1.26.10^7 & 7.19.10^7 & 1.7.10^7 \end{bmatrix}$$

Finally, the state feedback matrix of equation (24) is found by substituting matrices (20) and (23) in (10):

(24) $$K_a = [0.0507 \quad -0.2878 \quad -68.36]$$

DC-AC converter

The DC-AC converter used in this work is a full-bridge inverter with a coupling inductor at the output, as shown in Fig. 7. Inductor is the coupling element of the DC-AC inverter with the utility grid. Voltage source is the electric grid and resistor and inductor represent the resistance and inductance of the electric grid at coupling point. The input of the DC-AC converter is the DC-link shared with the DC-DC converter. The DC-link is represented by the C_{DC} capacitor.

The controller of the DC-link voltage provides the reference for the control of the output current of the inverter. A PLL (*phase-locked loop*) system (not shown in this paper) provides a sinusoidal waveform synced with the grid voltage. This waveform is used with the amplitude signal from the DC-link voltage controller for generating the output current reference.

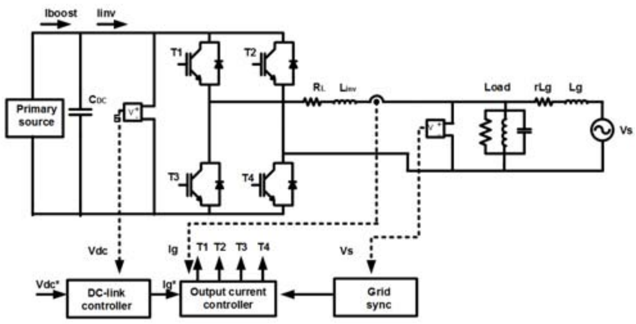

Fig. 4: Grid-connected DC-AC inverter

Modeling of the DC-AC converter

The aim of modeling the DC-AC converter, which is a full-bridge inverter, is obtaining a transfer function that will be useful for the design of the output current controller. The DC-link voltage is split in two halves and a virtual central point is established in the modeling process. In the following equations, voltages V_{t1} and V_{t2} are the voltages at the output terminals of the DC-AC full-bridge inverter. The transfer function of output current of the single-phase DC-AC inverter is expressed as (25), where V_{t1} is the inverter output voltage and I_{inv} is the output current injected into the utility grid.

(25) $$I_{inv}(s)\left(\frac{sL + R_L}{2}\right) = V_{t1} - \frac{V_s}{2}$$

In the transfer function of equation (7) only the voltage of one inverter output terminal is shown (V_{t1}) . This means that only one inverter leg is considered in the modeling process. The other leg, whose output voltage V_{t2} is controlled in a complementary way.

Considering the power injected into the DC-link, i.e. in the input of the DC-AC inverter, is a disturbance, once can neglect this disturbance and the transfer function of equation (26), which is the transfer function of the DC-link voltage regarding the injected power:

$$\frac{V_{dc}{}^2(s)}{P_{dc}(s)} = -\frac{2}{sC} \tag{26}$$

DC-AC converter control

Fig. 5 shows the control scheme of the DC-AC inverter. The square of the measured DC-link voltage is compared with the square of the voltage reference $(V_{dc}{}^*)^2$. The resulting error signal is compensated by the compensator $C_V(s)$. The output of the compensator is the power reference P_{ref} , which is used for generating the amplitude of the output AC current injected into the utility grid. The output current amplitude is calculated by dividing P_{ref} by the peak of the grid voltage V_S.

The value of the amplitude of the AC current multiplies a sinusoidal waveform obtained from a PLL system. The result of this multiplication is the current reference, i_g^* which is fed into the current control loop for generating the error signal from the comparison with the current measured at the output of the inverter. The current error is processed by the compensator *$G_C(s)$*, which provides the voltage reference *U'* for the full-bridge DC-AC inverter. Reference *U* is used in a PWM generator for generating the switching pulses of the inverter switches.

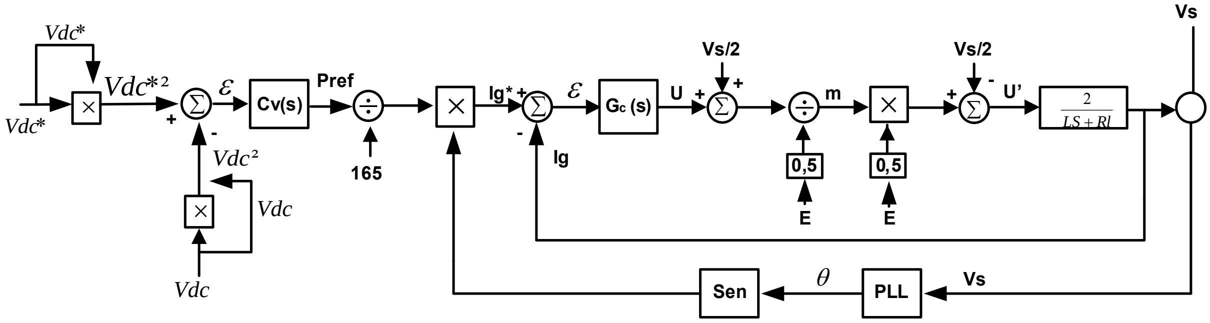

Fig. 5: Control system of the DC-AC inverter with a compensator for the control of the DC-link voltage and a compensator for the control of the sinusoidal AC output current. A PLL system is used for generating the reference of the output current.

One can see in the control scheme of Fig. 5 the presence of several feedwordard inputs with the grid voltage (V_S) and the DC-link voltage (*E*). The feedforward technique [3] helps to reduce the control effort and also in this case helps to decouple the control loop from the AC grid voltage.

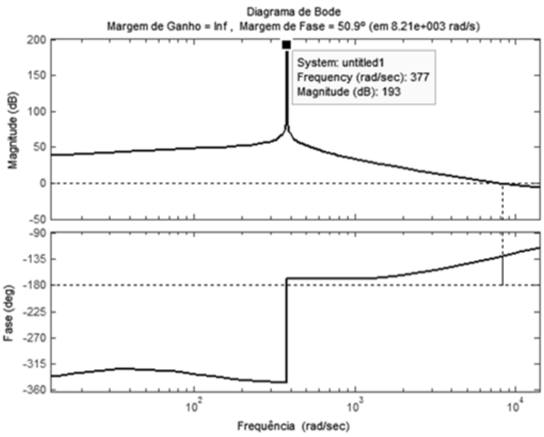

Fig. 6: Bode plot of the frequency response of the DC-AC current control system using a P+R compensator.

The current control loop *$G_C(s)$* is a P+R (proportional and resonant) compensator and the voltage compensator *$G_V(s)$* is a lead compensator. Fig. 9 shows the frequency response of the current control loop with compensator *$G_C(s)$*, where a resonance at frequency 377 rad/s may be noticed. The resonant frequency was chosen to be the same frequency of the AC grid voltage so that the current control system may achieve zero steady state error when synthesizing 60 Hz AC currents.

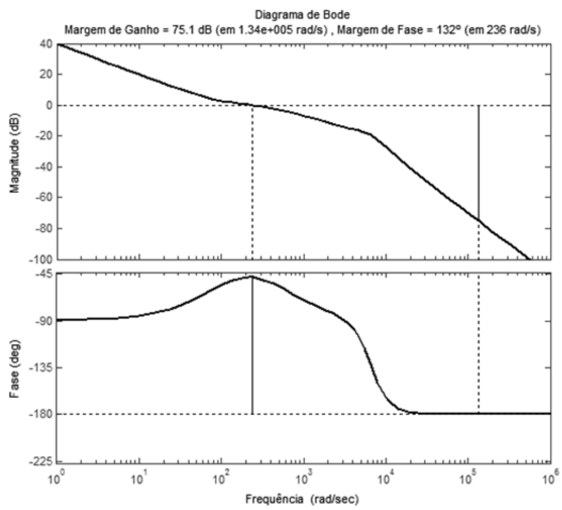

Fig. 7: Bode plot of the DC-link voltage control system using a lead compensator.

The Bode plot of Fig. 6 shows the system is stable with a margin phase of 50,9º. Fig. 7 shows the frequency response of the voltage control system with compensator *$G_V(s)$*, where a margin phase of 132 º makes the system stable.

Experimental results

The microinverter prototype shown in Fig. 8 was buit and the control systems designed in the preceding sections were implemented with the TMS320F28335 microcontroller. Fig. 9 shows the waveforms of the photovoltaic voltage (input of the DC-DC converter, channel #1) and of the AC current injected into the grid (chanel #2, 100 mV/A).

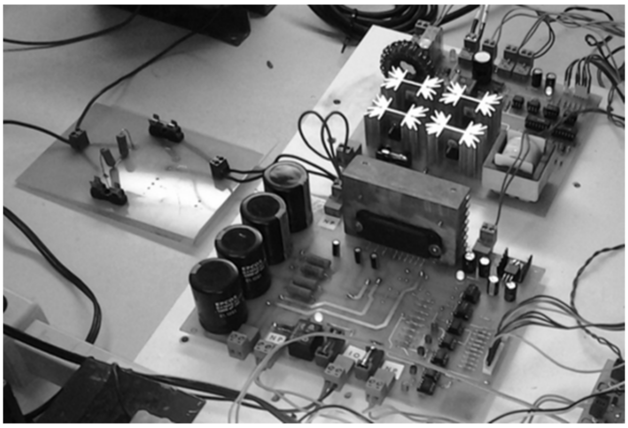

Fig. 8: Microinverter prototype

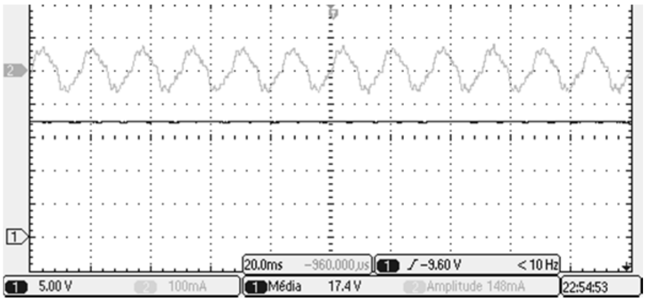

Fig. 9: Voltage at the output of the PV module (ch. 1) and current injected into the AC grid (ch. 2, 100 mV/A).

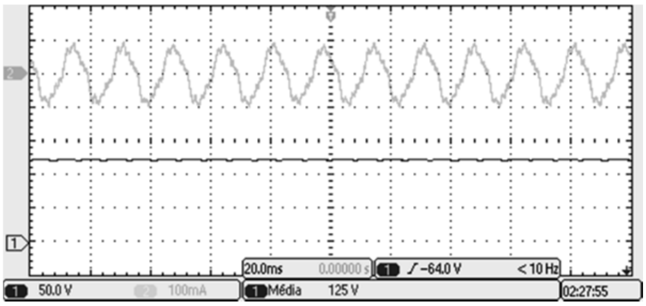

Fig. 10: DC-link voltage (ch. 1) and current injected into the AC grid (ch. 2, 100 mV/A).

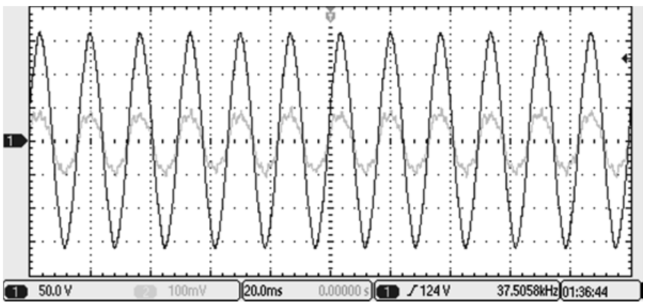

Fig. 11: Output current of the inverter (injected into the grid) and AC grid voltage.

Fig. 10 shows the voltage of the DC-link (channel #1) and the output AC current of the inverter injected into the grid (channel #2). One can see that the DC-link voltage remains constant no matter how much power is generated by the PV module. The extra energy injected into the DC-link by the DC-DC converter causes the output current of the DC-AC inverter increase, thus increasing the output power and making the power balance remain null at the DC-link. Fig. 11 shows the output AC current (channel #2) and the AC grid voltage (channel #1), both in perfect sync, which results null displacement factor and power factor near unity.

Conclusions

This work presented the development of a single-phase microinverter for grid-tie PV systems composed of two conversion stages: an isolated full-bridge DC-DC converter with high frequency transformer and a full-bridge DC-AC inverter attached to the grid with a coupling inductor. The DC-DC stage uses a high-frequency transformer that makes the inverter small and yet provides galvanic isolation from the grid, which is preferred in most PV systems. This microinverter allows the construction of versatile PV systems where each PV module is individually attached to the grid with a dedicated inverter. This increases the performance of PV systems by allowing individual maximum power point tracking for each module, besides other advantages such as making PV systems easy to install and to expand. The paper shows the design of control systems employed in the DC-DC and DC-AC converters and presents experimental results obtained with the prototype inverter. The main contribution of this work is the detailed modeling of the converter, with mathematical models and transfer functions for the DC-DC and DC-AC converters, and the design of compensators for the control loops presented in the preceding sections. The DC-DC control system was designed with the stage-space

The authors thank the Conselho Nacional de Desenvolvimento Científico e Tecnológico (CNPq) and Fundação de Amparo à Pesquisa do Estado de São Paulo (FAPESP) and CPFL(Companhia Paulista de Força e Luz) for financial support.

REFERENCES

[1] M. G. Villalva, "Conversor Eletrônico de Potência Trifásico para Sistema Fotovoltaico Conectado à Rede Elétrica", (in Portuguese) (2010), *PhD Thesis, Universidade Estadual de Campinas, UNICAMP*. Campinas, Brazil.

[2] S. Jiang, D. Cao, Y. Li e F. Z. Peng, "Grid-Connected Boost-Half-Bridge Photovoltaic Microinverter System Using Repetitive Current Control and Maximum Power Point Tracking", (2011). *IEEE TPEL*, vol. 27.

[3] Q. Li e P. Wolfs, "A Review of the Single Phase Photovoltaic Module Integrated Converter Topologies with three Different DC Link Configurations", (2008), *IEEE TPEL*, vol. 23.

[4] H. Ertl, J. W. Kolar e F. C. Zach, "A Novel Multicell DC–AC Converter for Applications in Renewable Energy Systems",(2002). *IEEE Transactions on Industrial Electronics*, vol. 49.

[5] L. G. Junior, "Inversores Integrados Monofásicos Aplicados em Sistemas Fotovoltaicos com Conexão à Rede de Distribuição de Energia", (2011)*, Universidade Estadual Paulista (UNESP). Mrs. Thesis*, Ilha Solteira, Brazil.

[6] D. C.Martins, R. Demonti e I. Barbi, "Usage of the Solar Energy from the Photovoltaic Panels for the Generation of Electrical Energy", (1999), *INTELEC*, Copenhagen.

[7] J. R. Gazoli, "Microinversor Monofásico para Sistema Solar Fotovoltaico Conectado à Rede",(2011), *Universidade Estadual de Campinas (UNICAMP). Dissertação de Mestrado*, Campinas,.

[8] D. C. Rezende, R. S. Ferreira, S. C. Guimarães Junior e J. R. Camacho, "Uma Proposta de Técnica de Rastreamento de Máxima Potência de um Módulo Fotovoltaico",(in Portuguese),(2010) *XVIII Congresso Brasileiro de Automática*

[9] N. Femia, G. Petrone, G. Spagnuolo e M. Vitelli, "Optimization of Perturb and Observe Maximum Power Point Tracking Method", (2005), *IEEE TPEL*, vol. 20.

[10] L. R. Oliveira, P. S.Nascimento, T. A. S. Barros, M. G. Villalva, E. Ruppert, "Input Voltage Regulation of an isolated Full-Bridge Boost Converter Fed By A Photovoltaic Device With The State-

Space Feedback Control Method”, (2013), *Congresso Brasileiro de Eletrônica de Potência*.
[11] M. G. Villalva, E. Ruppert, “Analysis and simulation ofthe P&O MPPT algorithm using a linearized PV array model”, (2009). *IECON'09 35th Annual Industrial Electronics Conference of IEEE*, 231-236,
[12] D. Cao, S. Jiang, F. Z. Peng and Y. Li, "Low Cost Trnasformer Isolated Boost Half - bridge Micro-inverter for Single-phase Grid-connected Photovoltaic System," (2012), *Applied Power Electronics Conference and Exposition (APEC)*, 2012 Twenty-Seventh Annual IEEE.
[13] P. de A. Sobreira, M. G. Villalva, P. G. Barbosa, H. A. C. Braga, J. R. Gazoli, E. Ruppert, A. A. Ferreira, Comparative analysis of current and voltage-controlled photovoltaic maximum power point tracking, Brazilian Power Electronics Conference (COBEP), 2011.
[14] P.Surma " A comparison between P&O and Fuzzy Logic methods for tracking the maximum power point," (2014), *Przegląd Elektrotechniczny*.
[15] A.Krupa, J.Dawidziuk, ‘High efficiency isolated DC/DC boost converter with planar magnetics for photovoltaic application’, (2014) *Przegląd Elektrotechniczny*, vol.7.
[16] M. G. Villalva, J. R Gazoli, E Ruppert, ‘Modeling and circuit-based simulation of photovoltaic arrays’, (2009), *Power Electronics Conference*,. COBEP'09. Brazilian, 1244-1254.
[17] R. W. Erickson, D. Maksimovic, Fundamentals of power electronics, (2001).
[18] M. G. Villalva, J. R. Gazoli, E Ruppert, “Comprehensive approach to modeling and simulation of photovoltaic arrays”, (2009) *Power Electronics, IEEE Transactions on* ,24 (5), 1198-1208,.
[19] N. S. Nise, Control Systems Engineering, (2010), Wiley.
[20] K. Ogata, Modern Control Engineering, (2002) Prentice Hall.

Authors:
Leonardo Ruffeil de Oliverira, Tárcio André dos Santos Barros, Paulo Sergio Nascimento Fo, Marcelo G. Villalva, Ernesto Ruppert. Av. Albert Einstein 400, Campinas, SP, Brasil,
E-mails: leo_ruffeil@hotmail.com, tarcioandre@hotmail.com, paulosnf@gmail.com,marcelo@fee.unicamp.br,ruppert@fee.unicamp.br